International Journal of Heat and Mass Transfer 97 (2016) 412–421

Contents lists available at ScienceDirect

International Journal of Heat and Mass Transfer

journal homepage: www.elsevier.com/locate/ijhmt

Nonlinear thermal parameter estimation for embedded internal Joule heaters

Abbas Tutcuoglu [a,b,c], Carmel Majidi [a,*], Wanliang Shan [a,d,*]

[a] Department of Mechanical Engineering, Carnegie Mellon University, Pittsburgh, PA 15213, USA
[b] Department of Aeronautics, Imperial College London, London, UK
[c] Département de Mathématiques et Informatique, École Centrale de Lyon, Ecully, France
[d] Department of Mechanical Engineering, University of Nevada, Reno, NV 89557, USA

ARTICLE INFO

Article history:
Received 17 September 2015
Received in revised form 9 February 2016
Accepted 9 February 2016
Available online 27 February 2016

Keywords:
Inverse heat conduction problem
Internal Joule heating
Adjoint method

ABSTRACT

We propose a novel inverse scheme, which allows for estimation of thermal parameters of internal Joule heaters through measurements of surface temperature distributions during a Joule heating process. The inverse scheme is based on the governing nonlinear, inhomogeneous heat conduction and generation equation and solely assumes knowledge of the electric resistivity of the Joule heater. Polynomial forms are assumed for the thermal conductivity $\kappa = \kappa(T)$ and $c_p\rho =: \lambda = \lambda(T)$, while the method can be easily generalized to estimate parameters of any suitable form. Both the sensitivity and the adjoint methods are developed and compared. Owing to the ill-conditioning of the inverse scheme, the performance of relaxation methods and regularization schemes are analyzed (to improve numerical conditioning). A verification was conducted using polydimethylsiloxane (PDMS) embedded with a strip of conductive propylene-based elastomer (cPBE). Good agreement was achieved between theoretical predictions by the inverse scheme and experimental measurements regardless of the approximated effective potential difference across the cPBE. While constant parameter estimations sufficed to approximate one reference temperature, the inclusion of multiple instants of time required an increase in the polynomial order. The improved parameter estimation is shown to remain of the same order of magnitude for the temperature range encountered when compared with the constant approximation, i.e. $\kappa = 10.7$ and 12.0 W m^{-1} K^{-1}, and $\lambda = 19.9$ and 16.2 J m^{-1} K^{-1}, respectively.

1. Introduction

Phase change and glass transition are typically used to enable rapid changes in the elastic rigidity of soft bio-inspired systems. Examples include PVAc–nanowhisker composites [1], shape memory polymer [2], wax [3], and conductive propylene-based elastomer (cPBE) composed of a percolating network of CB microparticles in a propylene–ethylene co-polymer [4]. In the case of cPBE, electrical current is applied to heat the composite above its glass transition temperature and to induce mechanical softening. Because of the low glass transition temperature T_g (~75 °C), activation can be achieved within a few seconds. However, further progress depends on improved electro-thermo-elasto characterization of the composite and surrounding insulating materials. Knowing parameters like specific heat c_p, density ρ and thermal conductivity κ allows for predictive modeling that can be used to identify material compositions and geometries that reduce electrical power requirements and activation time.

Here, we examine the thermal response of a general case of elastomeric composites illustrated in Fig. 1. The thermal phenomena under investigation are governed by the following transient heat conduction equation:

$$\rho(T)c_p(T)\frac{\partial T}{\partial t} = \frac{\partial}{\partial x}\left\{\kappa(T)\frac{\partial T}{\partial x}\right\} + q(T), \tag{1}$$

where T denotes temperature and $q(T)$ denotes the voltage dependent nonlinear heat generation and x denotes the spatial n-dimensional variable. We derive the adjoint equation for this method and compare it with the sensitivity-matrix-based approach. For the latter, different regularisation schemes are analyzed in order to improve the conditioning of the inversion of the sensitivity matrix. Relaxation methods are analyzed for both approaches. In order to obtain solutions for the direct scheme, a hybrid finite

* Corresponding authors at: Department of Mechanical Engineering, University of Nevada, Reno, NV 89557, USA (W. Shan).
E-mail addresses: abbas.tutcuoglu11@imperial.ac.uk (A. Tutcuoglu), cmajidi@andrew.cmu.edu (C. Majidi), wshan@unr.edu (W. Shan).

http://dx.doi.org/10.1016/j.ijheatmasstransfer.2016.02.015
0017-9310/

difference method (FDM) is applied, combining the merits of both implicit and explicit FDMs.

As shown in Fig. 1, the material of interest is embedded in PDMS, which has known physical parameters for the temperature range considered in this study. We will demonstrate that by embedding the material in PDMS, the precision of the emissivity matrix as recorded by a thermal microscope *Infrascope* (see Fig. 2b) can be considerably augmented. Internal Joule heating is presented as a novel tool to permit inverse determination of the thermal parameters of the material under investigation and possibly their temperature dependence. It is shown that this is only permissible for small enough heat generations, since otherwise, diffusion effects are difficult to capture and thus the estimation of such parameters becomes highly ill-conditioned.

Section 2 presents previous achievements in the field of inverse schemes particularly with respect to heat conduction as well as the motivation behind the novel inverse scheme. The subsequent section treats the underlying theory of the inverse scheme, including a discretized version of the governing PDE, the sensitivity and adjoint method and methods to improve the conditioning of the inherently ill-conditioned inverse scheme. A method to experimentally validate the applicability of the inverse scheme is given in Section 4 alongside the physical theory on which it is based. In Section 5, the inverse scheme's performance is first assessed in a theoretical one-dimensional framework, before the two-dimensional case is analyzed. These results are also compared with results from the experimental validation section. Finally, conclusions together with suggestions on how the scheme can be improved in the future is finally given in Section 6.

2. Background

Estimation of thermal parameters for new, sparsely studied materials is vital for numerous applications. Historically, these include space-related problems [5], the testing of components used in nuclear reactors [6,7] and temperature control for heat-treatment-based manufacturing processes such as quenching [8]. A more specific field of application consists in the control of the boundary temperature around Joule heaters, as depicted in [4] to allow close interaction with human skin. While for some of these applications it suffices to find a constant value invariant of space, time or any thermodynamic state, other materials show nonlinear behavior and hence complicate the search for these properties. While the determination of temperature distribution via knowledge of the governing parameters is referred to as the *direct problem*, the estimation of parameters via knowledge of the temperature distribution at discrete time points on a subset of the spatial domain is termed the *inverse problem* or alternatively, in the specific case of thermal conduction dominated environments, the *inverse heat conduction problem* (IHCP). Since small variations in the observed data, i.e. the temperature distribution on parts of the spatial domain, can lead to large variations in the estimation of the parameters, the inverse problem is ill-conditioned in essence. Noise within the given data is therefore unfavorable and to be kept at a minimum, as far as the nature of the experimental apparatus and its inherent imprecision permit.

Throughout the past decades, numerous inverse schemes have been proposed, which vary both in the methods applied as well as the restrictions and limitations imposed on the model. A fundamental categorization classifies schemes as either stochastic (e.g. [9–11]) or gradient based (e.g. [12–15]). This paper concentrates on the latter, of which the utmost part, as the name indicates, is based on an iterative process, in which the estimated parameters are steadily improved by determining the gradient and starting from an initial, to a certain degree arbitrary guess. The majority of methods can be categorized with respect to the means employed to obtain the gradient. The sensitivity method (e.g. [16–19]) is based on a numerical determination of the dependence of an incremental change in one of the parameters on the temperature distribution and thus evaluates the optimal gradient. The system of equations to be solved is ill-conditioned, but can be regularized using schemes such as L^2-regularization [20], Tykhonov-L^1 [21] or TSVD [22]. An alternative is given by the so-called adjoint method, which is based on the solution of the adjoint equation of the governing partial differential equation [23]. Even if the direction of the gradient obtained using one of the above methods reliably indicates the direction of steepest descent and hence an improved agreement between observation and simulation, the gradient's magnitude generally remains to be optimized. Although the scaling is usually highly case-specific, established methods exist, which hold across a diverse field of applications (see e.g. [24]). Methods differ in the assumption of the representation of the parameters. While functions free of assumptions on the functional form exist, other approaches assume polynomial or other suitable functional forms. The dependence itself further varies from case to case in that the independent variables comprise space or time and in other cases temperature itself.

Although numerous methods solving inverse problems based on reference data on the boundary have been presented throughout the past few decades (see e.g. Alfanov et al. [25]), a significantly smaller number of investigations addressing the experimental means of obtaining the boundary temperature is currently present. A classical means consists in simply heating one of the surface by a given heat flux and then determining the parameters from measurements on the boundary, as presented by Beck [26]. Hon [27] as well as Alifanov [12] investigated the IHCP involving the estimation of a boundary flux given the temperature distribution on a subset of the spatial domain. The case in which temperature measurements on the object are impractible is addressed by Howell [28], who uses remote measurements to apply an inverse method to estimate the radiative thermal properties. Owing to the ill-conditioned nature of the IHCP, issues with the precision of the transferred energy via external means can arise. This includes, for example, the extent to which hotplates can maintain a certain temperature to a constant level.

3. Theory on direct and inverse schemes

3.1. Finite difference scheme for nonlinear diffusion equations

Since for simple geometries, finite difference-based schemes provide sufficient accuracy together with low computational cost, the gain in accuracy via finite volume schemes, both fixed in order or of arbitrary order of accuracy, does not stand in relation to the increase in computational cost. The main challenge in constructing a stable and accurate scheme for the nonlinear heat-transport equation presented in Eq. (1) lies in the temperature-dependence of the parameters. While both transient and generation terms can be discretized at the N_x+1 nodes of a grid $\tau_n = \{x_i \,|\, i \in \{0,1,\ldots,N_x+1\} \subset \mathbb{R}, N_x \in \mathbb{N}$, where x_i denotes the position of node i, the conduction term requires the introduction of an additional interface grid $\tau_i = \{x_{i-1/2} \,|\, i \in \{0,1,\ldots,N_x+2\}\} \subset \mathbb{R}$ with $x_{min} = x_{-1/2} = x_0 < x_1 < x_{3/2} < \ldots < x_N < x_{N+1/2} < x_{N+1} = x_{N+3/2} = x_{max}, (x_{min}, x_{max}) \in \mathbb{R}^2$. The full grid containing both nodes and interfaces is denoted $\tau := \tau_n \cup \tau_i$.

In favor of a generalized approach, allowing explicit, semi-implicit as well as implicit treatments of the time-derivative, the following scheme is introduced [29]:

$$T_i^{n+1} = T_i^n + \frac{\theta\Delta t}{\Delta x \lambda_i^{n+1}}\left\{\kappa_{i-1/2}^{n+1}\frac{T_{i-1}^{n+1}-T_i^{n+1}}{\Delta x} + \kappa_{i+1/2}^{n+1}\frac{T_{i+1}^{n+1}-T_i^{n+1}}{\Delta x}\right\} + \frac{(1-\theta)\Delta t}{\Delta x \lambda_i^{n}}\left\{\kappa_{i-1/2}^{n}\frac{T_{i-1}^{n}-T_i^{n}}{\Delta x} + \kappa_{i+1/2}^{n}\frac{T_{i+1}^{n}-T_i^{n}}{\Delta x}\right\} + \Delta t(\theta s_i^{n+1} + (1-\theta)s_i^n), \quad (2)$$

where $\lambda := c_p\rho$. Unlike their linear counterparts, nonlinear partial differential equations do not allow for recovering explicit stability conditions via von Neumann schemes. Yet, by adopting a linearized approach, the following stability condition can be derived:

$$\frac{\Delta t}{\Delta x^2}\left\{\frac{(1-\theta)\kappa_{i,min}^n}{\lambda_i^n} - \frac{\theta\kappa_{i,min}^{n+1}}{\lambda_i^{n+1}}\right\} \leqslant \frac{1}{2}, \quad (3)$$

which shows that the fully-implicit version with $\theta = 1$ is unconditionally stable under the linearization.

3.2. Gradient-based inverse scheme

Prior to presenting the scheme, the functional form for the parameters to be estimated, namely λ and κ, is chosen to be polynomial. For different levels $l \in \{1,\dots,N\}$, where N is the highest order of the polynomials, the coefficients are contained in a vector $\mathbf{p} \in \mathbb{R}^{2l}$. The general form is given as $\mathbf{p} = [p_{\lambda,1},\dots,p_{\lambda,l},p_{\kappa,1},\dots,p_{\kappa,l}]^T$. The scheme used throughout this analysis is to a great extent based on the general outline of the gradient schemes used in [16,17]. Let $\mathcal{D} \subset \tau$, represent the discretized subdomain of the boundary on which temperature is measured, let $\tilde{\mathbf{T}} \in \mathbb{R}^{\tilde{n}\tilde{m}}$, where $\tilde{n} = |\mathcal{D}|$, and $\tilde{m} = |t_{rec}|$ for $t_{rec} \subset (0, t_{end})$, be the measured or observed temperature distribution and let $\mathbf{T}^k \in \mathbb{R}^{\tilde{n}\tilde{m}}$ denote the numerically determined temperature estimation using FDM at the same recording times $t \in t_{rec}$ and discretized subdomain $\mathcal{D}$. Finally, let the intermediate estimation of parameters be denoted by $\mathbf{p}_k$. A multi level approach will be used to gradually improve the estimation of the parameters as follows:

Let $l = 1$
Define initial linear parameter estimation $\mathbf{p}_0$
While $l \leqslant N$
  $k = 1$, $\mathbf{p}_k = \mathbf{p}_0$
  While $k \leqslant k_{max}$ *and* $E_k \geqslant \sigma_E$
    Use $\mathbf{p}_k$ *to obtain* $\mathbf{T}^k$
    Apply (*a*) *sensitivity based approach or*
    (*b*) *adjoint method to obtain* $\Delta\mathbf{p}^k$
    Apply relaxation to $\mathbf{p}_k$ *to obtain* r_k
    $\mathbf{p}_{k+1} = \mathbf{p}_k + r_k\Delta\mathbf{p}$
    $E_{k+1} = ||\tilde{\mathbf{T}} - \mathbf{T}^k||_2$
    $k := k + 1$
  $k := k - 1$
  $\mathbf{p}_0 = [p_{k_1} \cdots p_{k_l}\ 0\ p_{k_{l+1}} \cdots p_{k_{2l}}\ 0]^T$
$\mathbf{p} = \mathbf{p}_k$

3.2.1. Sensitivity-based approach

In this approach, the sensitivity of the measured temperature with respect to variations in the coefficients is quantified and summarized using a sensitivity matrix $\mathbf{J} = \partial\mathbf{T}/\partial\mathbf{p}$, which has the following form:

$$\mathbf{J} = \frac{\partial\mathbf{T}}{\partial\mathbf{p}}\bigg|_{\mathbf{p}_k} = \begin{bmatrix} \frac{\partial T_1}{\partial p_{\lambda,1}} & \frac{\partial T_1}{\partial p_{\lambda,2}} & \cdots & \frac{\partial T_1}{\partial p_{\kappa,l}} \\ \frac{\partial T_2}{\partial p_{\lambda,1}} & \ddots & \cdots & \cdots \\ \cdots & \cdots & \ddots & \cdots \\ \frac{\partial T_{\tilde{m}\times\tilde{n}}}{\partial p_{\lambda,1}} & \cdots & \cdots & \frac{\partial T_{\tilde{m}\times\tilde{n}}}{\partial p_{\kappa,l}} \end{bmatrix} \quad (4)$$

Given the measured temperature distribution, the change in parameters optimally has the following form:

$$\forall s \in \{1,\dots,\tilde{n}\times\tilde{m}\} : \tilde{T}_s - T_s^k = \sum_{i=1}^{l}\{\mathbf{J}_{s,i}\Delta p_{\lambda,i} + \mathbf{J}_{s,l+i}\Delta p_{\kappa,i}\} \iff \tilde{\mathbf{T}} - \mathbf{T}^k = \mathbf{J}\Delta\mathbf{p}, \quad (5)$$

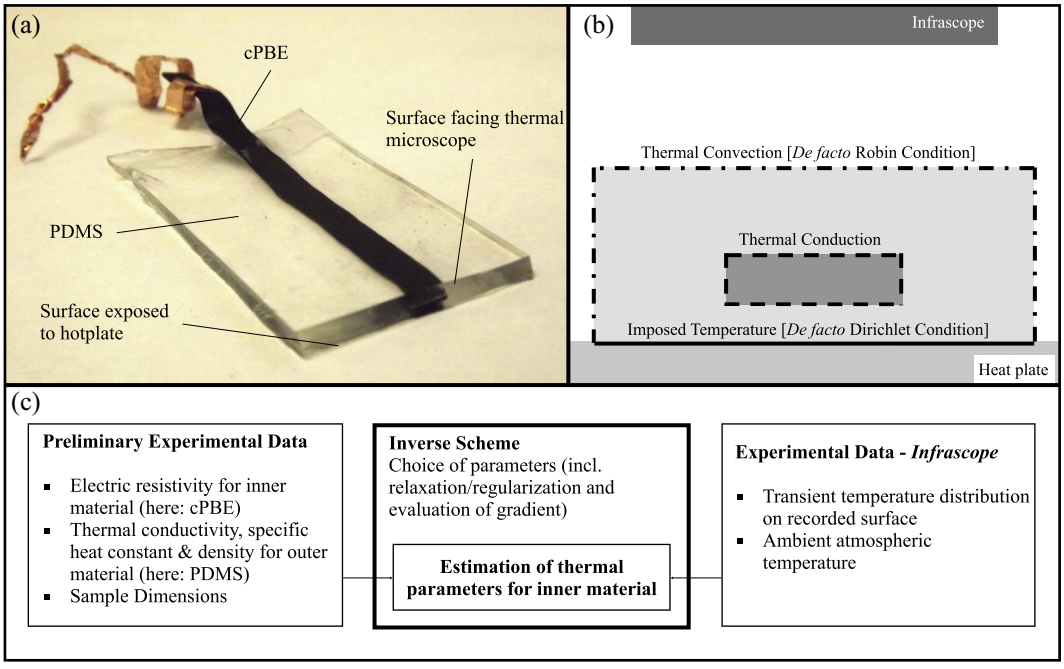

Fig. 1. (a) Image of cPBE-PDMS sample cut on a plane normal to the direction of the current. (b) Illustration of thermal boundary conditions based on sectional view of cut plane. (c) Fundamental functionality of proposed inverse scheme.

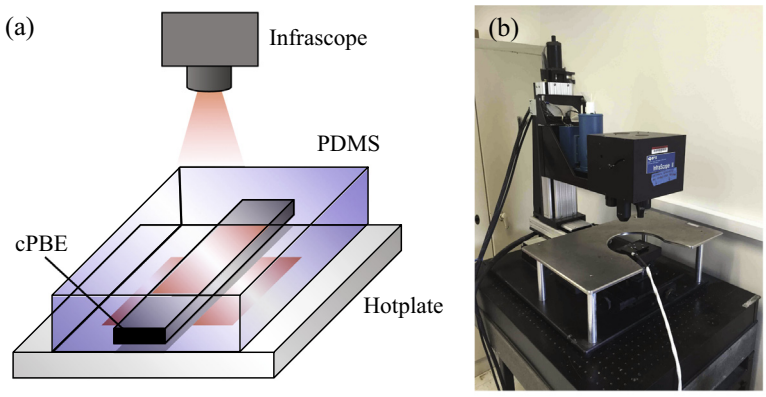

Fig. 2. (a) Sketch of the experimental apparatus and illustration of the *Infrascope*'s temperature measuring functionality. (b) View of *Infrascope* and hotplate.

where $\Delta\mathbf{p} = [\Delta p_{\lambda,1}, \ldots, \Delta p_{\lambda,l}, \Delta p_{\kappa,1}, \ldots, \Delta p_{\kappa,l}]^T$. In many cases, $\mathbf{J}$ is either non-invertible or ill-conditioned, and thus the original problem is replaced by the corresponding minimization problem

$$\Delta\mathbf{p} \in \underset{\Delta\hat{\mathbf{p}}\in\mathbb{R}^{2l}}{\text{Arg min}} \left\| \left[\tilde{\mathbf{T}} - \mathbf{T}^{\mathbf{k}}\right] - \mathbf{J}\Delta\hat{\mathbf{p}} \right\|_2, \quad l \in \{1, \ldots, N\}. \tag{6}$$

Based on the discrete L^2 norm, the new minimization problem is also referred to as L^2 regularization. It can be shown that the above problem has an exact analytic solution (see e.g. [30]):

$$\Delta\mathbf{p} = (\mathbf{J}\mathbf{J}^T)^{-1}\mathbf{J}^T\left\{\mathbf{T} - \mathbf{T}^{\mathbf{k}}\right\} \tag{7}$$

A closely related version of the above minimization problem is formed by including a penalization factor of the gradient. Using the L^1 norm, multiplied by some penalization constant $\sigma_{TKH} \in \mathbb{R}^+$ can potentially prevent the gradient from having an excessive magnitude, but can also lead to a loss of information via over-regularisation. The right choice of the penalization constant is thus vital [31]. The L^1-regularized, or Tykhonov-regularized minimization problem as well as its exact analytic solution are given as:

$$\Delta\mathbf{p} \in \underset{\Delta\hat{\mathbf{p}}\in\mathbb{R}^{2l}}{\text{Arg min}} ||[\tilde{\mathbf{T}} - \mathbf{T}^{\mathbf{k}}] - \mathbf{J}\Delta\hat{\mathbf{p}}||_2 + \sigma_{TKH}||\Delta\mathbf{p}_k||_1,$$
$$l \in \{1, \ldots, N\} \Rightarrow \Delta\mathbf{p} = (\mathbf{J}\mathbf{J}^T - \sigma_{TKH}\mathbf{I})^{-1}\mathbf{J}^T\left\{\mathbf{T} - \mathbf{T}^{\mathbf{k}}\right\} \tag{8}$$

In certain cases, the L^2 regularization can be improved by inserting a preliminary TSVD-regularization. This is expected to become increasingly useful for highly ill-conditioned schemes.

3.3. Adjoint method

The central idea behind the adjoint method, as it is used in this context, lies in using a scalar objective function $E = E(\mathbf{p}, \mathbf{T})$ and a set of governing equations $\mathbf{H}(\mathbf{p}, \mathbf{T}) = \mathbf{0}$ such as to form an adjoint equation to $\mathbf{H}$. Starting from the first variation in E and $\mathbf{H}$:

$$\delta E = \left[\frac{\partial E}{\partial \mathbf{p}}\right]^T \delta\mathbf{p} + \left[\frac{\partial E}{\partial \mathbf{T}}\right]^T \delta\mathbf{T}, \quad \delta\mathbf{H} = 0 = \left[\frac{\partial \mathbf{H}}{\partial \mathbf{p}}\right]\delta\mathbf{p} + \left[\frac{\partial \mathbf{H}}{\partial \mathbf{T}}\right]\delta\mathbf{T} \tag{9}$$

and via introduction of a Lagrange-multiplier ϕ, the following equation can be deduced:

$$\delta E = \left\{\left[\frac{\partial E}{\partial \mathbf{p}}\right]^T + \phi^T\frac{\partial \mathbf{H}}{\partial \mathbf{p}}\right\}\delta\mathbf{p} + \left\{\left[\frac{\partial E}{\partial \mathbf{T}}\right]^T + \phi^T\left[\frac{\partial \mathbf{H}}{\partial \mathbf{T}}\right]\right\}\delta\mathbf{T}. \tag{10}$$

Since ϕ is unknown, δE will be independent of $\delta\mathbf{T}$ and solely dependent on variations in $\mathbf{p}$ by setting the term preceding $\delta\mathbf{T}$ equal to zero. We demonstrate the adjoint-method via its application to the problem of the nonlinear IHCP at hand. Let

$$E(\mathbf{p}, T) = \frac{1}{2}\int_\Omega \int_0^{t_{end}} |T(x,t) - T^*(x,t)|^2 dxdt \tag{11}$$

and let H be the set of governing equations with initial temperature T_0 and boundary conditions $g(T, \partial T/\partial x) = 0$. The adjoint equation is then given by:

$$\begin{cases} -\lambda\frac{\partial\phi}{\partial t} - \frac{\partial}{\partial x}\left[\kappa\frac{\partial\phi}{\partial x}\right] + \frac{\partial\kappa}{\partial T}\frac{\partial T}{\partial x}\frac{\partial\phi}{\partial x} - \frac{\partial q}{\partial T}\phi = 0 \quad \forall(x,t) \in \Omega \times (0, t_{end}), \\ \phi(x, t_{end}) = T(x, t_{end}) - T^*(x, t_{end}) \quad \forall x \in \Omega, \\ g^T\left(\phi, \frac{\partial\phi}{\partial x}\right) = 0 \quad \forall(x_{\partial\Omega}, t) \in \partial\Omega \times (0, t_{end}), \end{cases} \tag{12}$$

where $g^T(\phi, \partial\phi/\partial x)$ depends on $g(T, \partial T/\partial x)$, i.e. the boundary conditions for the original problem. Table 1 summarizes the form of g for Dirichlet, Neumann and Robin boundary conditions.

Having obtained the distribution of ϕ on $\Omega \times (0, t_{end})$ and under the assumption that the temperature dependence of the parameters is given by polynomials of order N_s, $s \in \{\lambda, \kappa, q\}$, we obtain:

$$\nabla_{p_s} s = \left[1, T^1, \ldots, T^{N_s}\right]^T. \tag{13}$$

The gradient is thus given as:

$$\nabla p := \begin{bmatrix} \nabla p_\lambda \\ \nabla p_\kappa \\ \nabla p_q \end{bmatrix} = \int_\Omega \int_0^{t_{end}} \begin{bmatrix} \phi\frac{\partial T}{\partial t}\nabla_{p_\lambda}\lambda \\ \frac{\partial\phi}{\partial x}\frac{\partial T}{\partial x}\nabla_{p_\kappa}\kappa \\ -\phi\nabla_{p_q}q \end{bmatrix} \tag{14}$$

with $\nabla p \in \mathbb{R}^{|\Delta p_\lambda| + |\Delta p_\kappa| + |\Delta p_q|}$. While the above derivation is based on a continuous spatial and temporal domain, the discontinuous implementation is accomplished via an explicit finite difference scheme and the gradient is obtained via the simple trapezoidal rule. The above form of the gradient shows, that the adjoint method is expected to become computationally less expensive than the sensitivity method for increasing numbers of parameters, since the latter requires n_p simulations for n_p configurable parameters, while the adjoint method requires the solution of only one finite value problem (FVP).

Table 1
Form of $g^T(\phi, \partial\phi/\partial x)$ depending on boundary condition of the original problem.

Boundary condition	$g(T, \partial T/\partial x)$	$g^T(\phi, \partial\phi/\partial x)$
Dirichlet	$T\|_{\partial\Omega}$	$\phi\|_{\partial\Omega}$
Neumann	$\frac{\partial T}{\partial x}\|_{\partial\Omega}$	$\frac{\partial\phi}{\partial x}\|_{\partial\Omega}$
Robin	$\kappa(T)\frac{\partial T}{\partial x}\|_{\partial\Omega} - h(T_a - T\|_{\partial\Omega})$	$h\phi\|_{\partial\Omega} - \frac{\partial\phi}{\partial x}\|_{\partial\Omega}$

3.4. Relaxation methods

Having obtained the gradient direction, its optimal length or in other terms, the scaling or relaxation factor r^k, remains to be determined. The first and simplest approach is given by a constant relaxation factor. For applications where there exists no *a priori* knowledge of the size of the gradient, the constant relaxation factor approach becomes difficult to deal with, because too large gradients can cause divergence away from the minimum and too small gradients require high numbers of iterations. Since the corresponding minimization problem is solely one-dimensional, in the sense that the relaxation factor is a scalar, an optimization approach is feasible as a second approach. Local minima can cause problems. However, since for a given set of parameters these would most likely also arise for the aforementioned method, they do not weaken the position of the optimal approach. For regions without an *a priori* knowledge on the magnitude of the gradient, it provides a reliable approach and can in special cases even lower the computational effort, which might otherwise be incurred by a small gradient size and thus high numbers of iterations. A third approach extends the first approach by an adaption of the relaxation factor: if the error decreases, no changes are made; if however, the error increases, r^k is scaled down.

4. Experimental validation

For the experimental validation of the proposed scheme, temperature data obtained via the thermal microscope *Infrascope*, presented in Section 4.1, is used. Prior to the recording of measurements, liquid nitrogen is added to the infrascope to minimize noise in the measurements. Underneath the lense, which can be adjusted to attain the best possible resolution for the surface to be recorded, a hotplate is used to impose a *de facto* Dirichlet condition on the bottom of the sample under investigation. The hotplate can also initially help to reduce noise, in that the sample can be brought to a temperature at which environmental radiation from the surrounding can be neglected. For this experiment, an initial temperature of 49.5 °C is found to achieve relatively low noise.

The sample consists of the aforementioned cPBE embedded into PDMS. Fig. 2 illustrates the experimental apparatus. The cPBE is situated 0.95 mm above the hotplate with another 1.77 m to the upper surface of the PDMS and 13.8 mm and 12.6 mm to the PDMS' two lateral surfaces. The cPBE strip itself has dimensions of 0.61 mm height and 3.2 mm width. The two ends of the cPBE outside the PDMS region are connected via aluminum foil to a power source. A voltage of 72.5 V is then applied across the two ends and measurements taken at an interval of 5 frames over a total of 150 frames with a rate of approximately 0.84 frames per second. While λ_{PDMS} is assigned the same value as in Section 5.2, κ_{PDMS} is set to 0.75 W m^{-1} K^{-1}. The discrepancy to established values from literature is discussed later. Two cases are analyzed: The former solely considers the results at 89.8 s, whereas the latter refers to three recordings from t$\in$ {28.0 s,59.8 s,89.8 s}. With reference to Section 5.2, uncertainty in contact resistance has been taken into account prior to running the model, by testing for an effective potential difference of 85%, 90%, 95% and 100% of the targeted voltage. Table 6 summarizes the coefficients obtained for the λ and κ approximation as constants and 1st order polynomials for each of the aforementioned voltages. The results for the linear case are illustrated in Fig. 5.

4.1. Infrascope measurements

Infrascope is a thermal microscope. Prior to taking any measurements, an emissivity matrix is recorded, by imposing a temperature on the sample or a subdomain of the sample. Applying Stefan–Boltzmann law

$$Q = \epsilon\sigma' T^4 \tag{15}$$

and including the energy measurements of the infrared radiation, Q, of the sample at interest as well as the Boltzman constant σ', the emissivity ϵ can be deduced. The desired temperature for this step can be achieved via a hotplate, integrated in the *Infrascope* apparatus. However, convection of the sample's surface exposed to air can cause a non-zero temperature gradient, and thus an erroneous emissivity matrix. Inaccuracy of the hotplate in maintaining a constant level of temperature can accentuate this phenomenon. Furthermore, a significant temperature gradient through the different layers can be observed, since the surface has to arrive at a temperature high enough to distinguish its radiation from natural radiation, in this context also referred to as noise. In order to minimize this potential source of error, we make use of the transmittance property of PDMS, which is elaborated in Section 4.2. Without an *a priori* estimation of the thermal conductivity – which would be needed to infer a steady-state temperature distribution – employing more PDMS above than underneath the cPBE brings the true temperature at the reference surface closer to the targeted temperature. Because of the aforementioned transmittance, the PDMS between the recorded and exposed surfaces barely affects the quality of the image and instead results in a gain in accuracy.

4.2. Transmittance of PDMS

Several studies have been conducted on the transmittance of PDMS with regard to near-IR and IR radiation (see e.g. [32–34]). In [32], De Groot proposed to make use of the significant transmittance for waveguide applications. He traces the high transmittancy rate in this particular region of wavelengths back to vibrational absorbance and further mentions the low refraction rate of about 1.40–1.42 for PDMS as well as the low scattering thanks to its homogeneity. Chen et al. further analyzed potential influence factors such as the mixing ratio of base to curing agent and the purge time and concluded, that the transmittance rate for the range of IR-wavenumbers that they analyzed is equal and superior to 50% [33]. Whitesides and Tang used the same properties for fluidic optics [34]. All three conclusions justify the experimental apparatus elaborated in Section 4.1.

5. Results and discussion

Having established a theoretical foundation on the inverse determination of the polynomial representation of $\kappa(T)$ and $\lambda(T)$, we now proceed to analyze both sensitivity- and adjoint-method-based approaches. While experimentally acquired data will be of central importance in Section 5.3, prior verification of the functionality of the two proposed schemes and the effectiveness of regularisation as well as relaxation methods is required. Unless otherwise specified, all benchmarks are based on a spatial domain spanning $[-5,+5]$ with 24 interior discretization points. The time after which the temperature distribution is recorded is set to $t = 0.5$. The corresponding interval is represented by 2000 equispaced time-steps.

5.1. Comparison of sensitivity and adjoint method-based approach

A first comparison study is conducted between the sensitivity and the adjoint method. In order to assess estimations, the given temperature distribution is associated to the exact parameters given by $\kappa(T) = 1$ and $\lambda(T) = 1.05$. Running both sensitivity with

L^2-regularisation and the adjoint-method based schemes then yielded the results in Fig. 3.

While both approaches set the relaxation factor to a constant value of $r_0 = 1.0$, the sensitivity-based approach proves to converge after significantly less iterations. This can potentially be traced back to the missing regularization in the case of the adjoint method and thus the deteriorating effect of a badly conditioned system. Alternatively, a CFL number close to 0.5 and the choice of an explicit scheme enhances the transient error transport, which could explain the offset of the gradient from the optimum direction.

As mentioned in Section 3, regardless of the number of parameters N, the adjoint method requires no more than one solution to the FVP at hand as opposed to N solutions to the direct problem for the sensitivity method to estimate the local gradient. Thus, it is expected that at least from a computational cost point of view, the merits of the adjoint method unclose for $N \gg 1$. Simultaneously, a rising number of parameters can lead to the formation of local minima. This principle and the subsequent ill-conditioning, which expresses itself in the form of an increased susceptibility of the final minimum with respect to the initial conditions, is illustrated in Fig. 4 as observed in the case of the adjoint method.

5.2. Numerical analysis of feasibility of the proposed apparatus and scheme

The proposed scheme to obtain transient measurements on the surface of cPBE, allowing the simultaneous determination of both κ and λ, is analyzed with regards to its susceptibility to potential environmental factors. These factors include the uncertainty in the contact resistance, which can effectively lead to an overestimation of the potential difference along the sample, the emissivity rate for the surface of the cPBE, normally distributed noise, and the applicability of the assumption that the surrounding medium's governing thermal parameters are temperature-invariant.

Uncertainty in contact resistance: While an initially sufficiently high pressure on the electrodes connected to the cPBE can minimize the contact resistance, the onset of glass transition, i.e. softening of the material can lead to a deterioration of the contact and thus an increase in the contact resistance. This in return decreases the effective voltage and therefore automatically the heat generation as well. Table 2 summarizes the results for a constant effective voltage deficit. While this does not capture the temperature-dependent onset of contact loosening, it admits insights into the susceptibility. It is found that even for 45 V, i.e. 50% of the effective voltage as compared to the total potential difference applied to the circuit, the estimation for the conductivity coefficient is still found in the same order of magnitude as the corresponding exact parameter. On the other hand, λ, yields a more susceptible nature with a high offset already at 67.5 V, i.e. 75% of the targeted voltage. This is accredited to the influence of λ on the spatial transport of the generated heat: as noise attains a high enough level to make it impossible to reach certain data points via the current heat generation available, λ explodes such as to magnify the effect of q on $\partial T/\partial t$.

Uncertainty in the emissivity: The procedure outlined in Section 4, contained an initial calibration in order to obtain the emissivity matrix associated to the spatial area recorded. Due to potential offsets of the measured temperature to the objective temperature during calibration, as well as partial absorption of the radiation by the PDMS, the emissivity values are expected to bear uncertainty. Table 3 illustrates the result from the following analysis: five sets of given temperature are created, with initial temperature $T_{init,k} = \phi_k \times 50\,^{\circ}\mathrm{C}$, with $\phi_k = 0.95 + (k-1) * 0.025$, $k \in \{1, \ldots, 5\}$. The respective solutions T_k are computed and divided by ϕ_k, in order to obtain the expected observed temperature fields under the assumption of an unchanged shift factor. Parameter estimations in the same order of magnitude as the exact parameters are obtained for $\phi_1, \phi_2, \phi_3, \phi_4$. Albeit expectations of the parameter estimation deteriorating with increasing uncertainty in the emissivity, an improved parameter estimation was obtained for $\phi_1 = 0.95$ as compared to $\phi_2 = 0.975$.

Normally distributed noise: Noise is apparent in all systems, but can have varying levels of influence. Since inverse schemes are ill-conditioned, the scheme's susceptibility with respect to a normally distributed, unbiased noise is analyzed for standard deviations ranging from scales as small as 0.001 to higher magnitudes of 0.1. Table 4 shows how well the L^2 regularization embedded in the sensitivity-based approach regularized the noise. Further regularization schemes, such as the Tykhonov L^1 regularization, which complements the least square approach by a penalty term, were taken into consideration but did not show any significant merit, regardless of the order of magnitude of the standard deviation. While the average estimation of parameters shows small susceptibility, provided a sufficiently high number of trials, the standard deviation in the parameter estimation – while not becoming excessively large – increases.

Uncertainty in the thermal parameters of the surrounding medium: Based on the higher glass transition temperature of PDMS or potential substitutes the respective thermal parameters are assumed to be constant. The effect of potential variations of these

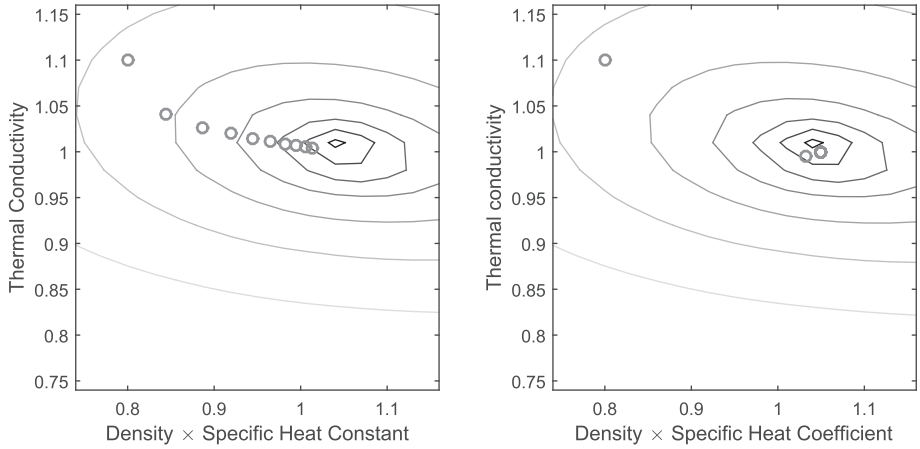

Fig. 3. Comparison of (a) the adjoint-method and (b) the sensitivity-approach equipped with L^2-regularisation, for a constant parameter representation and without relaxation.

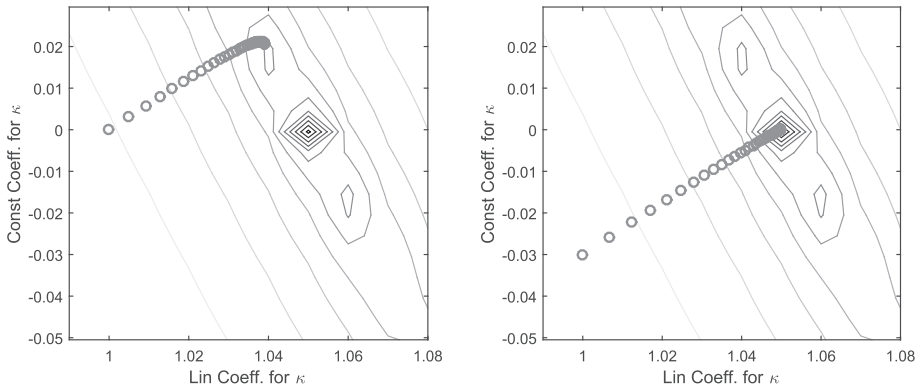

Fig. 4. Illustration of convergence towards different local minima via shift of initial parameter estimation.

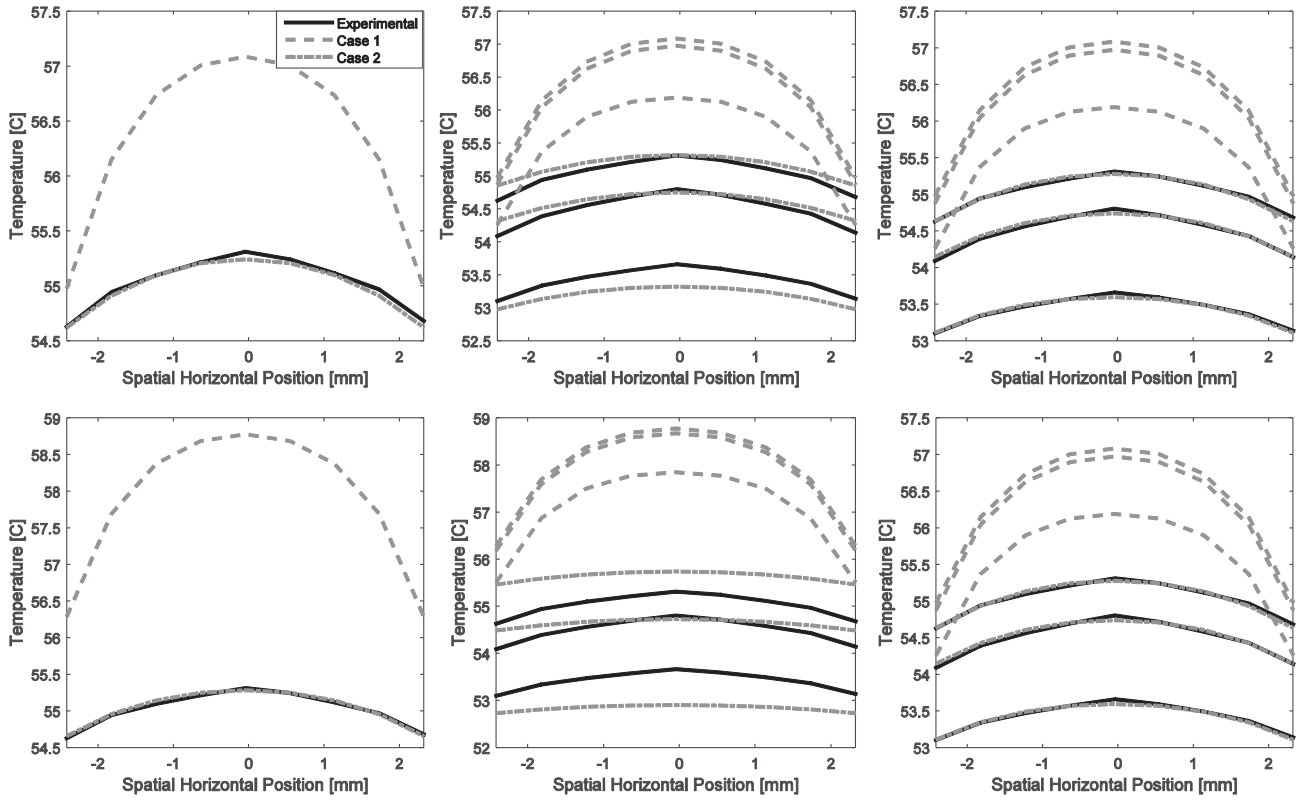

Fig. 5. Comparison between the experimental temperature distribution (*black*) and the numerical temperature distribution, based on either the same physical parameters of cPBE as for PDMS (*Case 1*) or optimized parameters following the employment of the inverse scheme (*Case 2*). The effective potential differences are 85% (*top*) and 100% (*bottom*) of the targeted voltage.

parameters on the estimation of the parameters of cPBE is of interest. A two-dimensional domain is introduced with the spatial domain spanning $\Omega = [-15\text{ mm}; +15\text{ mm}] \times [0; 3.3\text{ mm}]$ and $\Omega_{cPBE} = [-2.2\text{ mm}; +2.2\text{ mm}] \times [0.9\text{ mm}; 1.6\text{ mm}] \subset \Omega$ representing the cPBE-containing domain. The simulation holds at $t = 168$ s and records the temperature at the upper PDSM-cPBE interface $\partial\Omega_{PDMS} \cap \{y = 1.6\text{ mm}\}$ every 8 s after the start. The exact thermal parameters of cPBE and PDMS are set to $\kappa_{cPBE} = 1.0\text{ W m}^{-1}\text{ K}^{-1}$, $\lambda_{cPBE} = 1.0 \times 10^{+6}\text{ J m}^{-1}\text{ K}^{-1}$, $\kappa_{PDMS} = 1.5\text{W m}^{-1}\text{ K}^{-1}$ and $\lambda_{PDMS} = 1.5 \times 10^{+6}\text{J m}^{-1}\text{ K}^{-1}$. The values for PDMS are chosen in accordance with [35]. The temperature dependence of the electric resistivity used to determine the electric resistance is based on the values given in [4], a voltage of 90 V and a sample length of 13 cm. Table 5 presents the results after the parameters κ_{PDMS} and λ_{PDMS} are multiplied by three different factors 0.75, 1.00 and 1.25 to obtain the reference temperature distributions. The inverse scheme is run with the unmodified values to simulate the effect of uncertainties. While for the selected values, all estimations lie within the same order of magnitude, it can be inferred, that overestimating the real value of either parameter has a higher impact than an underestimation.

5.3. Application of the scheme to experimental measurements

Qualitatively, it can be observed that a zeroth order approximation suffices to numerically yield a temperature distribution close to the data from the *Infrascope* if only one reference recording is considered, regardless of the voltage considered. Large discrepancies between the numerical and experimental results are observed for the case of three reference recordings. Because the coefficients

Table 2
Variation of the L^2 error ($\times 10^{-5}$) of the given and estimated temperature field and the two parameters κ ($\times 10^{-1}$) and λ ($\times 10^{6}$) with effective voltage V across the specimen.

Effective voltage	$L^2(T)$ ($\times 10^{-5}$)	p_λ	p_κ
45.0	120.0	35806.3	9.1
67.5	52.2	13.5	6.2
81.0	14.1	7.5	2.7
90.0	0.0	1.0	1.0

Table 3
Mean and maximum L^2-error of the temperature field, as well as mean parameter estimation and corresponding L^1 error with respect to the exact parameters $\kappa = 1.0 \times 10^{-1}$ and $\lambda = 1.0 \times 10^{+6}$.

Shift factor	$L^2(T)(\times 10^{-5})$	p_λ	p_κ
0.950	108.1	0.4	0.5
0.975	49.3	0.4	0.1
1.000	0.3	1.0	1.0
1.025	27.1	11.7	2.6
1.050	59.6	185.4	5.5

stay constant across all temperatures, there exists no set of parameters via which the L^2 error converges to *zero*. An increase of the polynomial order to *one* already allows to obtain a good agreement.

Quantitatively, it can be observed that despite a convergence of the L^2 error, the parameters obtained for different voltages largely differ. This is an immediate consequence of varying heat generations, which in return requires to reduce or increase the heat flux to PDMS in order to attain the experimentally observed temperature distribution. The effect is particularly emphasized for the first order approximation of the physical parameters. Computing the estimated physical quantities in the interval $T \in \{49.5\,^\circ\text{C}, 55.5\,^\circ\text{C}\}$, it can be observed that the estimated parameters for the zeroth order approximation are situated in the respective intervals. This in return justifies the motivation of this inverse scheme, particularly with regards to the improvements to the case with three reference distributions achieved via an increase of the order of the polynomial.

Although convergence was found in two cases, residual errors persist. The origin of these could lie in reference distributions that cannot be reproduced via zeroth or first order approximations. Reasons different to the order of magnitude that could simultaneously cause the observed discrepancy in parameters are found in the aforementioned difference in effective applied voltage between the two ends of the cPBE. Since the λ obtained for the zeroth order approximation with one reference distribution predominantly fall into the respective parameter interval spanned by the first order approximation over $T \in \{49.5\,^\circ\text{C}, 55.5\,^\circ\text{C}\}$ for the same voltage and because the κ barely change, a rough estimation of the contact resistance would lead to significantly improved estimations. Alternatively, a non-uniform current density across the cross-section of the cPBE sample could cause a spatially varying heat generation. The uncertainty in the estimation of the heat generation term of PDMS is a potential error source as well. Because of a current lack of information on the dependence of the physical parameters of PDMS on the volumetric fractions of its constituents, its thermal conductivity had to be roughly estimated. Adopting a thermal conductivity close to the value given in [35] leads to a high heat transfer from the cPBE to PDMS, which results in too low temperature distributions across the cPBE sample. In such a case, the inverse scheme is not able to find a set of parameters that replicates the experimental measurements without a significant error. This is expected to stem from a potential discrepancy in the volumetric

Table 4
Mean and maximum L^2-error of the temperature field, as well as mean parameter estimation and corresponding L^1 error with respect to exact parameters $\kappa = 1.0 \times 10^{-1}$ and $\lambda = 1.0 \times 10^{+6}$.

$\overline{L^2(T)}$ ($\times 10^{-5}$)	$\max L^2(T)$ ($\times 10^{-5}$)	p_λ	$\overline{E_{p_\lambda}}$ ($\times 10^{-5}$)	$\max E_{p_\lambda}$ ($\times 10^{-5}$)	p_κ	$\overline{E_{p_\kappa}}$ ($\times 10^{-5}$)	$\max E_{p_\kappa}$ ($\times 10^{-5}$)
0.96	1.15	0.98	0.018	0.046	0.98	0.022	0.060
1.96	2.34	0.97	0.035	0.106	0.96	0.047	0.111
9.75	11.04	0.98	0.106	0.200	0.95	0.095	0.182

Table 5
Variation of the L^2 error ($\times 10^{-5}$) of the given and estimated temperature field (*left*) and the two estimated parameters p_κ (*center*) and p_λ (*right*) with modulation of κ (*column-wise constant*) and λ (*row-wise constant*).

Factor	**0.75**	**1.00**	**1.25**
0.75	40.04	38.54	60.91
1.00	1.11	0.03	1.22
1.25	13.30	13.34	13.41

Factor	**0.75**	**1.00**	**1.25**
0.75	0.36	0.37	0.01
1.00	0.98	1.00	1.03
1.25	6.09	6.12	6.17

Factor	**0.75**	**1.00**	**1.25**
0.75	0.09	0.41	0.00
1.00	0.37	1.00	1.54
1.25	1.15	1.87	2.54

Table 6
L^2-Error for 0th (*top*) and 1st (*bottom*) order polynomial approximations of κ and λ between the numerical and the experimental solution for $V_{eff} \in \{61.6, 65.3, 68.9, 72.5\}$ V. 0th order approximations are given for both the case of one (*top left*) and three (*top right*) reference temperature recordings.

V_{eff} [V]	$p_{\kappa,0}$ [$\times 10^{-3}$]	$p_{\lambda,0}$ [$\times 10^{6}$]	L_2 [$\times 10^{-4}$]	V_{eff} [V]	$p_{\kappa,0}$ [$\times 10^{-3}$]	$p_{\lambda,0}$ [$\times 10^{6}$]	L_2 [$\times 10^{-4}$]
61.6	12.3	10	1.72	61.6	19.5	8.07	23.4
65.3	12.2	14.3	1.29	65.3	26.7	10.8	43.3
68.9	11.9	18.3	1.18	68.9	15.3	14.5	58.7
72.5	11.6	22.3	1.32	72.5	41.3	16.3	71.8

V_{eff} [V]	$p_{\kappa,0}$ [$\times 10^{-3}$]	$p_{\kappa,1}$ [$\times 10^{-3}$]	$p_{\lambda,0}$ [$\times 10^{6}$]	$p_{\lambda,1}$ [$\times 10^{6}$]	L_2 [$\times 10^{-4}$]
61.6	11.3	0.00	−86.5	1.81	3.81
65.3	10.6	0.00	−183	3.71	4.59
68.9	0.00	0.184	−261	5.27	6.23
72.5	9.71	0.00	−331	6.68	8.18

fractions used within this experiment and the PDMS referred to in [35]. A value of $\kappa_{PDMS} = 0.75\text{W m}^{-1}\text{ K}^{-1}$ however restricted the heat flux and hence allowed to find sets of parameters replicating the experimental measurements. In future applications, it would be advisable to first employ a metal with known electric resistivity as the internal Joule heater to inversely determine κ_{PDMS} and λ_{PDMS}. Further improvements can be accomplished with regards to an appropriate choice of initial parameters. While the aforementioned technique of taking previous results from lower order approximations as initial conditions for higher order polynomials increases the likelihood of convergence, a global search algorithm is more reliable in finding the global minimum.

6. Conclusions

A novel method to inversely determine the physical parameters κ and λ of an internal Joule heater was presented. The theoretical background of the gradient-based inverse scheme with respect to the non-linear heat conduction and generation equation was demonstrated. A number of cases were analyzed, in which uncertainties were purposefully introduced to assess the eligibility of the proposed method in environments of great uncertainty. Alongside the mathematical foundation, the means of recording the temperature was explained in the special case of PDMS. Simultaneously, limitations were given with respect to the choice of the outer material surrounding the internal Joule heater.

The theory's applicability was then assessed in the framework of a practical case, in which cPBE as the internal Joule heater was embedded into PDMS. The temperature recordings were effectuated using the *Infrascope*. For the case of solely one reference temperature distribution, convergence in the sense of practically vanishing L^2 errors was shown. The computed parameters were however of limited use since only one temperature distribution was considered, although the main interest of the method lied in the determination of parameters valid throughout the full temperature range of the experiment. The subsequent inclusion of two further reference distributions resulted in a rise of the L^2-error and hence demonstrated that a constant parameter assumption is insufficient to model the thermal conductance over the entire temperature range. A linear approximation significantly improved the result, in that the L^2 error eventually adopted sufficiently small values. Minor residual errors were nevertheless present and a comparison of parameters obtained for different voltages showed significant discrepancies. To mitigate these effects, it was suggested to effectuate estimations of the contact resistance between cPBE and aluminum, to acquire more accurate data regarding thermal properties of PDMS and to critically assess the assumptions made with respect to the heat generation, in that the current density could be non-uniform across the cPBE-cross-section, despite direct current.

Acknowledgements

The authors acknowledge the financial support of DARPA Young Faculty Award (Grant # N66001-12-1-4255) for this work. The authors thank Dr. Shichun Yah at Mechanical Engineering Department at Carnegie Mellon University for providing access to *Infrascope*, Prof. Shlomo Ta'asan at the Department of Mathematical Science at Carnegie Mellon University for the helpful discussions on adjoint methods, and Mr. Amir Mohammodi Nasab at Mechanical Engineering Department at University of Nevada, Reno for helping run the simulations.

References

[1] J.R. Capadona, K. Shanmuganathan, D.J. Tyler, S.J. Rowan, C. Weder, Stimuli-responsive polymer nanocomposites inspired by the sea cucumber dermis, Science 319 (2008) 1370–1374.
[2] W. Shan, T. Lu, C. Majidi, Soft-matter composites with electrically tunable elastic rigidity, Smart Mater. Struct. 22 (8) (2013) 085005. <http://stacks.iop.org/0964-1726/22/i=8/a=085005>.
[3] W. Shan, T. Lu, Z. Wang, C. Majidi, Thermal analysis and design of a multi-layered rigidity tunable composite, Int. J. Heat Mass Transf. 66 (2013) 271–278, http://dx.doi.org/10.1016/j.ijheatmasstransfer.2013.07.031. <http://www.sciencedirect.com/science/article/pii/S0017931013005851>.
[4] W. Shan, S. Diller, A. Tutcuoglu, C. Majidi, Rigidity-tuning conductive elastomer, Smart Mater. Struct. 24 (6) (2015) 065001.
[5] E. Kudryavtsev, K. Chakalev, N. Shumakov, Transient Heat Transfer, Izd. Akad. Nauk SSSR, Moscow.
[6] B. Bass, Application of the finite element method to the nonlinear inverse heat conduction problem using becks second method, J. Manuf. Sci. Eng. 102 (2) (1980) 168–176.
[7] D. France, R. Carlson, T. Chiang, W. Minkowycz, Critical heat flux experiments and correlation in a long, sodium-heated tube, J. Heat Transfer 103 (1) (1981) 74–80.
[8] G. Stolz, Numerical solutions to an inverse problem of heat conduction for simple shapes, J. Heat Transfer 82 (1) (1960) 20–25.
[9] T. Butler, D. Estep, A numerical method for solving a stochastic inverse problem for parameters, Ann. Nucl. Energy 52 (0) (2013) 86–94, http://dx.doi.org/10.1016/j.anucene.2012.05.016. <http://www.sciencedirect.com/science/article/pii/S0306454912001806> (Nuclear reactor safety simulation and uncertainty analysis).
[10] T. Butler, D. Estep, J. Sandelin, A computational measure theoretic approach to inverse sensitivity problems II: a posteriori error analysis, SIAM J. Numer. Anal. 50 (1) (2012) 22–45, http://dx.doi.org/10.1137/100785958.
[11] J. Breidt, T. Butler, D. Estep, A measure-theoretic computational method for inverse sensitivity problems I: method and analysis, SIAM J. Numer. Anal. 49 (5) (2011) 1836–1859, http://dx.doi.org/10.1137/100785946.
[12] O.M. Alifanov, Inverse Heat Transfer Problems, vol. 1, Springer-Verlag, New York, 1994.
[13] C.-H. Huang, S.-P. Wang, A three-dimensional inverse heat conduction problem in estimating surface heat flux by conjugate gradient method, Int. J. Heat Mass Transf. 42 (18) (1999) 3387–3403, http://dx.doi.org/10.1016/S0017-9310(99)00020-4. <http://www.sciencedirect.com/science/article/pii/S0017931099000204>.
[14] M. Prud'homme, T. Nguyen, On the iterative regularization of inverse heat conduction problems by conjugate gradient method, Int. Commun. Heat Mass Transfer 25 (7) (1998) 999–1008, http://dx.doi.org/10.1016/S0735-1933(98)00091-8. <http://www.sciencedirect.com/science/article/pii/S0735193398000918>.
[15] D.N. Hào, H.-J. Reinhardt, Gradient methods for inverse heat conduction problems, Inverse Prob. Eng. 6 (3) (1998) 177–211.
[16] M. Cui, X. Gao, J. Zhang, A new approach for the estimation of temperature-dependent thermal properties by solving transient inverse heat conduction problems, Int. J. Therm. Sci. 58 (2012) 113–119, http://dx.doi.org/10.1016/j.ijthermalsci.2012.02.024. <http://www.sciencedirect.com/science/article/pii/S1290072912000786>.
[17] M. Cui, X. Gao, H. Chen, Inverse radiation analysis in an absorbing, emitting and non-gray participating medium, Int. J. Therm. Sci. 50 (6) (2011) 898–905, http://dx.doi.org/10.1016/j.ijthermalsci.2011.01.018. <http://www.sciencedirect.com/science/article/pii/S1290072911000275>.
[18] N.-Z. Sun, W.W.-G. Yeh, Coupled inverse problems in groundwater modeling: 1. sensitivity analysis and parameter identification, Water Resour. Res. 26 (10) (1990) 2507–2525.
[19] N.-Z. Sun, W.W.-G. Yeh, Coupled inverse problems in groundwater modeling: 2. identifiability and experimental design, Water Resour. Res. 26 (10) (1990) 2527–2540.
[20] A.Y. Ng, Feature selection, L^1 vs. L^2 regularization, and rotational invariance, in: Proceedings of the Twenty-first International Conference on Machine Learning, ACM, 2004, p. 78.
[21] A.N. Tikhonov, V.I. Arsenin, Solutions of Ill-posed Problems, Vh Winston, 1977.
[22] M. Migliaccio, S. Farris, M. Sunda, Tsvd regularization in inverse microwave radiometry problem, in: Geoscience and Remote Sensing Symposium, IGARSS '02, 2002 IEEE International, vol. 4, 2002, pp. 2559–2561. http://dx.doi.org/10.1109/IGARSS.2002.1026610.
[23] Y. Jarny, M. Ozisik, J. Bardon, A general optimization method using adjoint equation for solving multidimensional inverse heat conduction, Int. J. Heat Mass Transf. 34 (11) (1991) 2911–2919, http://dx.doi.org/10.1016/0017-9310(91)90251-9. <http://www.sciencedirect.com/science/article/pii/0017931091902519>.
[24] A. Belmiloudi, F. Mahé, On nonlinear inverse problems of heat transfer with radiation boundary conditions: application to dehydration of gypsum plasterboards exposed to fire, Adv. Numer. Anal. 2014 (2014). 18 pp. Article ID 634712.
[25] O.M. Alifanov, E.A. Artiukhin, S.V. Rumiantsev, Extreme Methods for Solving Ill-posed Problems with Applications to Inverse Heat Transfer Problems, Begell house, New York, 1995.
[26] J. Beck, B. Blackwell, A. Haji-Sheikh, Comparison of some inverse heat conduction methods using experimental data, Int. J. Heat Mass Transf. 39

(17) (1996) 3649–3657, http://dx.doi.org/10.1016/0017-9310(96)00034-8. <http://www.sciencedirect.com/science/article/pii/0017931096000348>.
[27] Y. Hon, T. Wei, A fundamental solution method for inverse heat conduction problem, Eng. Anal. Bound. Elem. 28 (5) (2004) 489–495, http://dx.doi.org/10.1016/S0955-7997(03)00102-4. <http://www.sciencedirect.com/science/article/pii/S0955799703001024> (Mesh reduction technique, Part 1).
[28] J.R. Howell, R. Siegel, M.P. Menguc, Thermal Radiation Heat Transfer, CRC Press, 2010.
[29] N. Ozisik, Finite Difference Methods in Heat Transfer, CRC Press, 1994.
[30] D. Joshi, Linear Estimation and Design of Experiments, New Age International Publishers, 1987.
[31] T. Zhang, Some sharp performance bounds for least squares regression with l1 regularization, Ann. Stat. 37 (5A) (2009) 2109–2144.
[32] R. De Jaeger, M. Gleria, Inorganic Polymers, Nova Science Pub Incorporated, 2007.
[33] K.-C. Chen, A.-M. Wo, Y.-F. Chen, Transmission Spectrum of PDMS in 4–7μm Mid-IR Range for Characterization of Protein Structure, vol. 2, 2006, p. 893. <http://www.nsti.org/procs/Nanotech2006v2/9/W61.502>.
[34] G.M. Whitesides, S.K.Y. Tang, Fluidic Optics, Proc. SPIE 6329, Optofluidics, 2006, http://dx.doi.org/10.1117/12.681672. 63290A.
[35] Massachusetts Institute of Technology – Material Property Database (PDMS). <http://www.mit.edu/6.777/matprops/pdms.htm> (accessed 16.9.2014).